Journal of
Ceramic Science
and Technology

J. Ceram. Sci. Technol., **11** [1] 1-10 (2020)
DOI: 10.4416/JCST2019-00031
available online at: http://www.ceramic-science.com

Investigation of Chemically Modified ICIE16 Bioactive Glass, Part II

F.J. Hmood*[1], F. Schmidt[2], O. Goerke[3], J. Günster[2]

[1]University of Babylon, Al Hillah, Babylon, Iraq
[2]BAM Bundesanstalt für Materialforschung und -prüfung, Unter den Eichen 87, D-12205 Berlin, Germany
[3]Technische Universitat Berlin, Straße des 17. Juni 135, D-10623 Berlin, Germany

received April 24, 2019; received in revised form August 15, 2019; accepted October 24, 2019

Abstract

Chemically modified bioactive glasses based on ICIE16 were prepared with the melt-quenching method using water as a quenching medium. The sinterability of these bioactive glasses was investigated and is discussed in this article. The sintering experiments were conducted with different sintering temperatures, sintering times and heating rates. Those parameters are crucial for dense glass with an amorphous structure. The particle size (d50) of the starting glass powder was determined at 88 μm and kept constant. The pre-pressed glass pellets were cold-isostatically pressed at 300 MPa to a green density of around 63 %. Density development, phase identification, shrinkage behavior and the microstructure were investigated to determine the sinterability of the developed glasses. The glass powders were sintered at different temperatures inside the processing window while crystallization was monitored. The results have shown that the sinterability of the developed glasses strongly depends on the proposed chemical additions. The highest density reached was 96 %, which belongs to BP1 glass with sintering conditions of 20 K/min heating rate for 60 min at 750 °C.

Keywords: Bioactive glass, viscous sintering, crystallization, processing window, grain boundary

I. Introduction

Silica-based bioactive glass is an interesting material for medical applications, especially for bone and bone tissue repair [1]. The well-known composition 45S5 bioglass® exhibits low sinterability, as it is prone to crystallization during densification. The apparent reason is that the glass has low viscosity in the sintering range in comparison to high-silica-content glass, for instance, soda-lime glass. 13 – 93 bioactive glass, which has a silica content of around 54 mol%, shows improved sinterability compared to the known Bioglass® [2].

In the first part of this study, the effect of modifying the chemical composition of ICIE16 bioactive glass on the processing window and the bioactivity were discussed in depth. The base composition of the ICIE16 is given in Reference [3]. With regard to chemical modifications, silica was partially replaced with boron, while calcium was partially replaced with magnesium. In addition, some of the soda was replaced with phosphorus pent oxide. It was anticipated that these changes would strengthen the glass network by increasing cross-linking in the silica network. According to the modifications, the designed glasses were divided into three groups, i.e. B, BP, and BM. The new compositions have shown moderate bioactivity in comparison to that of ICIE16 and 45S5 [4, 5]. More information is given in Reference [5].

In this article, the sinterability of the developed glasses – denoted B1, B2, B3, BP1, BP2, BP3, BM1, BM2, and BM3 – was investigated. The glass samples were sintered utilizing the viscous flow of glass. A global flow of material is necessary until full densification is reached without grain boundaries being retained between the sintered particles [6, 7]. One main set of parameters influencing glass sinterability is related to the powder particle features, such as particle size and surface topology of the particles. The other set of parameters is related to the sintering process conditions, this includes sintering temperature, sintering time, heating rate and the external pressure. In addition, the viscosity of glass being sintered, which is related to the glass composition, also has an influence on the glass sinterability [8, 9]. Another influencing factor may be the milling process itself and the milling media [10]. Generally, viscous sintering consists of three stages: Neck formation, global mass transportation and finally porosity closing [11]. In the first stage, neck areas form as the material is driven towards the particle contact points. During the second phase, a massive flow of material heads towards the neck areas, which is associated with continuous shrinkage. This shrinkage continues until the glass sintering is finished. This is unlike the sintering mechanism of crystalline ceramics where the diffusion of species controls the sintering process and the shrinkage occurs during the final stage of sintering [12].

Wu *et al.* tried to sinter ICEI16 glass to produce scaffolds with an amorphous structure by means of gel-casting. The glass was prepared with the melt-quenching method, then milled and finally formed with the gel-casting method. They reported that the glass can be successfully sintered at 700 °C for 60 min. The microstructure images showed

* Corresponding author: firas.hmood@googlemail.com

that the glass partially crystallized during the heat treatment into $K_3Na(SiO_4)_2$ and $Na_2CaSi_3O_8$, resulting in a glass-ceramic. Different parameters affected the resulting microstructure, these were the particle size, time of gelation, and gel-drying temperature [6].

The aim of this article is to investigate the sinterability of the developed bioactive glasses and to discuss the effect of the process parameters as well as the composition modifications on their sinterability. The processing parameters of interest in this study are temperature, dwell time, and the heating rate of the heat treatment.

II. Experiments

(1) Sample preparation

ICIE16 bioactive glass and nine modified glasses were synthesized. The chemical composition and the synthesis approach have been explained previously in Reference [5]. Glass pellets were formed by means of dry pressing. An amount of 0.1 g of each glass was pre-pressed in a hardened steel mold with an inner diameter of 6 mm at a pressure of 0.9 MPa for 10 min and then isostatically pressed at 300 MPa pressure. The final dimensions were 5.97 x 1.85 (D x h) mm. A resistance furnace (Nabertherm, Germany) was used for the heat treatment. The sintering conditions were chosen based on differential thermal analysis (409 STA, Netzsch-Germany).

(2) Characterizations

(a) *Particle size and density*

The particle size of the powders used was measured using a laser diffraction particle size analyzer (LS I3320, Beckman Coulter, Germany). This device measures in two measuring conditions wet and dry. In our case, the particle size of the glass powders was measured in wet condition. For dry conditions, it can measure from 0.004 nm to 2 000 nm, while for wet conditions, the measuring range is from 0.017 nm to 2 000 nm.

The density of the synthesized glasses (ρ_{glass}) was determined according to the Archimedes method. While the apparent density of the sintered glasses (ρ_{sin}) was calculated as mass to volume ratio. The volume was measured with a precise caliber and the mass with a digital balance (Sartorius, Germany). Densities are given as a ratio of sintered glass density to the density of the synthesized glass (ρ_{sin}/ρ_{glass}). The green density of the pressed glasses was about 63 %.

(b) *Sintering (shrinkage) behavior*

Shrinkage of the prepared bioactive glasses was measured in non-isothermal heat treatment performed using a hot-stage microscope (EMI 201 up to 1 600 °C, Hesse Instruments, Germany). The silhouette area of the sample was measured as a function of the sample temperature. The samples were heated from room temperature up to 1 100 °C at a heating rate of 10 K/min. All the experiments were conducted in normal atmosphere. Real-time images for the samples' silhouette area were recorded using a camera, which is aligned with the furnace and a halogen lamp. Alumina sample holders were used to support the glass samples during the heating cycles.

Utilizing the shrinkage information, isothermal heat treatment was conducted at 650, 700, 750, 800 °C. The dwell time was chosen to be 60 and 120 min at the respective sintering temperatures. In addition, the heating rates were 10 to 20 K/min. Heating rates higher than 20 K/min could not be realized with the resistance furnaces used. The samples were sintered in a normal atmosphere.

(c) *Phase identification*

The yield phases were investigated with the X-ray diffraction method. A D8 Diffractometer (Bruker, Germany) with CoKα radiation in Bragg-Brentano mode was used to record the X-ray diffraction. The scanning speed was set to 0.019 °/s. The crystal size of the new crystallites was determined utilizing the Scherrer equation ($\beta = \frac{k \cdot \lambda}{\zeta \cdot \cos\theta}$) as in [13], where β is the crystallite size in nm, k is the Scherrer constant (0.89), λ is the wavelength of Cokα(1.79 nm) and finally θ is the diffraction angle. Z is the line broadening at half the maximum intensity which was calculated for the highest peak intensity.

(d) *Microstructure*

A scanning electron microscope and energy-dispersive X-rays (SEM, Hitachi SU8030, Japan) were used to investigate the microstructure of the sintered samples. The scanning voltage was 15 kV and the current was 1 mA. The investigation was performed on fractured and polished surfaces. For polishing, the specimens were fixed in an epoxy bed, ground and eventually polished up to 1 µm grain size.

III. Results

(1) Sintering behavior

(a) *Non-isothermal sintering*

Fig. 1a shows the shrinkage behavior of the developed bioactive glass samples. In general, all the glasses showed a single shrinkage step except for ICIE16 glass, which showed two steps starting at 672 and 797 °C, respectively. B1 and B2 glasses started to shrink first at around 680 °C and stopped at around 780 °C. The shrinkage of the two glasses was determined as 26 % and 27 % respectively. The other glasses B3, BP1, BP2, BP3, BM1, BM2 and BM3 started to shrink at around 685 °C and stopped at 810 °C. These glasses had a final shrinkage of 32 %, 35 %, 32 %, 35 %, 32 %, 34 %, and 32 %, respectively. BP1, BP3 and BM2 glasses showed the biggest shrinkage with values of 34 % and 35 %, while ICIE16 showed a shrinkage of around 28 %.

The temperatures for shrinkage onset and end – determined with heating microscopy – correspond well with those determined with the DTA analysis. According to the DTA investigation, the crystallization process for most glasses starts between 800 and 850 °C, therefore we limited further sintering investigations to a maximum of 800 °C in this study. Sintering at higher temperatures will increase the formation of crystalline phases inside the amorphous matrix, which was not desirable in the scope of this study.

(b) ***Isothermal sintering***

In this part of the study the influence of dwell temperature, dwell time and heating rate was investigated. At 650 °C, 60 min dwell time, and a heating rate of 10 K/min, the density (ρ_{sin}/ρ_{glass}) is above 70 % for all the prepared glasses but ICIE16, which reached a density of 68 % (Table 1). Fig. 2 shows the density variation at 700 °C and 750 °C for one-hour dwell time. It is clear that 700 °C was insufficient to close all the voids in the glass compacts and hence they showed low density. Increasing the sintering temperature to 750 °C led to an increase in density for all the glasses to around 92 % except ICIE16, which showed a density of 85 % (Fig. 2a and 2b). At 800 °C, the density (Table 1) of the glass compacts does not change significantly compared to those sintered at 750 °C. Increasing the dwell time to 120 min at the same sintering temperatures and a heating rate of 10 K/min led to slight increases in the density of the sintered glasses (Table 1).

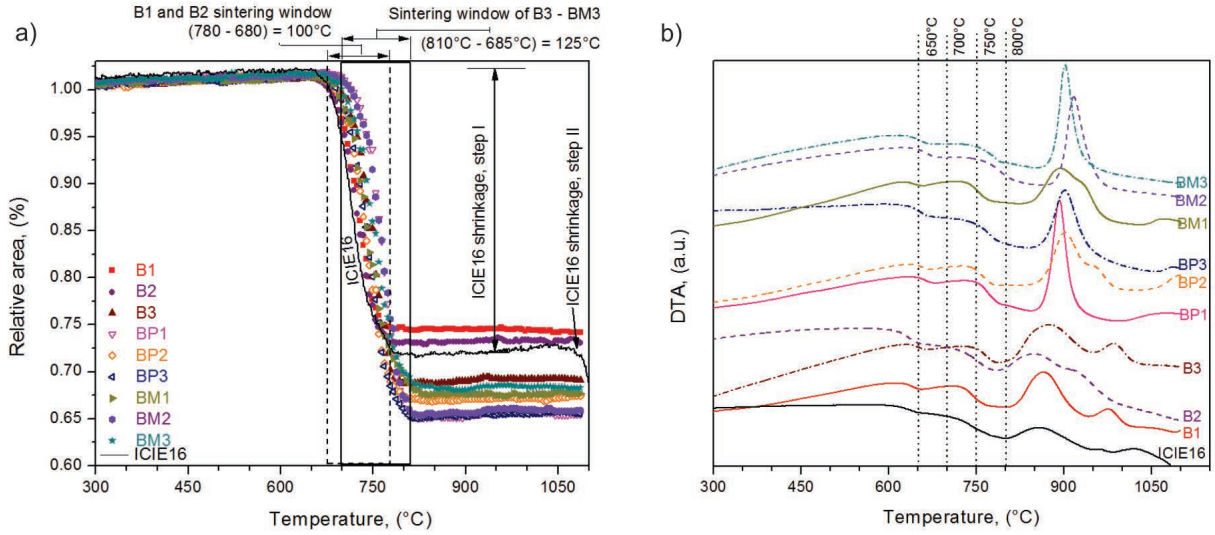

Fig. 1: a) Sintering behavior of the prepared bioactive glasses. b) DTA investigation of the same bioactive glasses. All the glasses start to sinter at around 680 °C, while they finish sintering at different temperatures depending on their chemical composition.

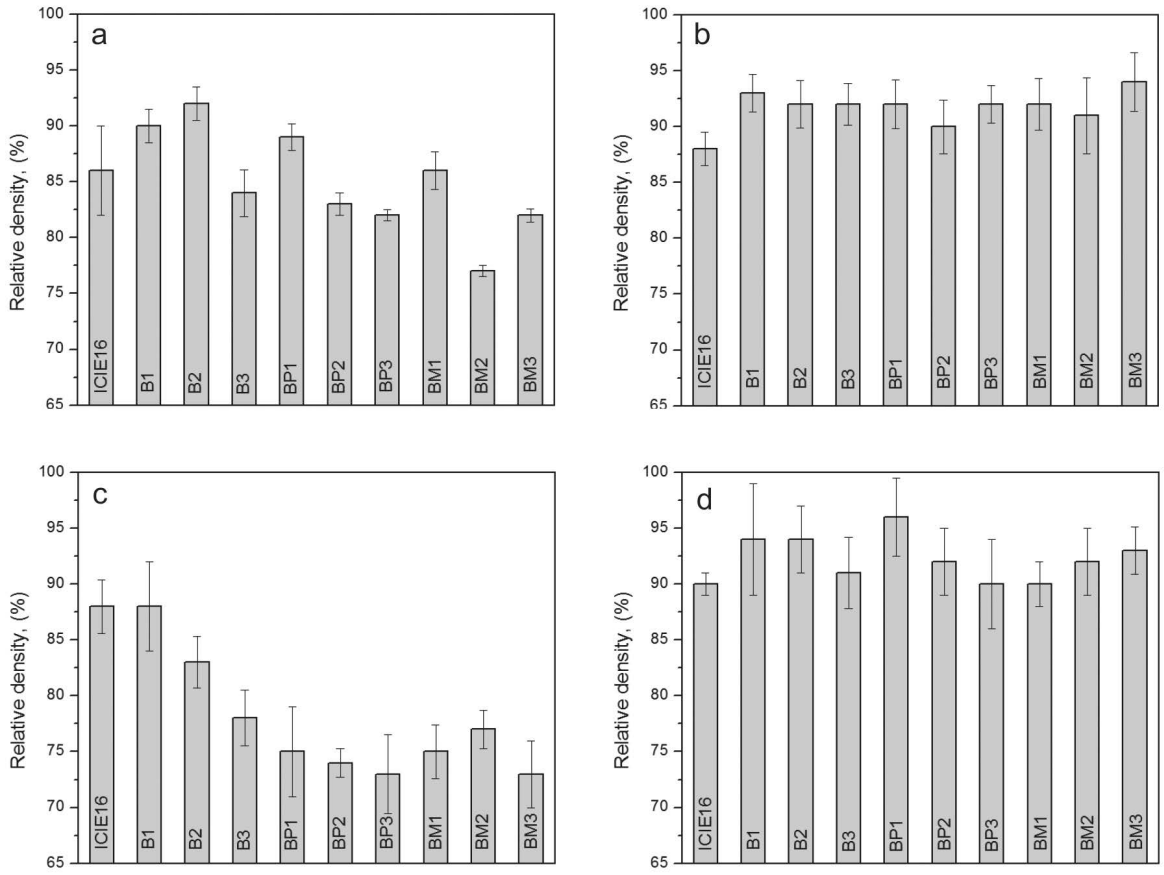

Fig. 2: Relative density of the sintered glasses. a) at 700 °C / 10 K/min / 60 min; b) at 750 °C / 10 K/min / 60 min; c) at 700 °C / 20 K/min / 60 min; d) at 750 °C / 20 K/min / 60 min.

Table 1: Results of density at a heating rate of 10 K/min and at dwell times of 60 and 120 min.

BG	T_{sin}, °C	Heating rate, K/min	Dwell time, min	ρ_{sin}, g/cm^3	density, %	Dwell time, min	ρ_{sin}, g/cm^3	density, %
ICIE16				1.890 ± 0.005	68		1.905 ± 0.006	68
B1				2.098 ± 0.018	76		2.119 ± 0.019	**77**
B2				2.004 ± 0.022	74		2.030 ± 0.028	75
B3				2.054 ± 0.027	74		2.076 ± 0.016	74
BP1	650	10	60	2.011 ± 0.005	72	120	2.033 ± 0.009	73
BP2				2.069 ± 0.011	74		2.090 ± 0.012	74
BP3				2.059 ± 0.012	73		2.084 ± 0.031	74
BM1				2.037 ± 0.018	73		2.086 ± 0.020	74
BM2				2.015 ± 0.005	72		2.060 ± 0.036	74
BM3				2.016 ± 0.012	73		2.053 ± 0.011	74
ICIE16				2.396 ± 0.040	86		2.438 ± 0.114	**88**
B1				2.478 ± 0.015	90		2.493 ± 0.009	90
B2				2.492 ± 0.015	92		2.513 ± 0.003	93
B3				2.342 ± 0.021	84		2.400 ± 0.004	86
BP1	700	10	60	2.475 ± 0.012	89	120	2.518 ± 0.007	90
BP2				2.327 ± 0.010	83		2.469 ± 0.008	**88**
BP3				2.302 ± 0.005	82		2.424 ± 0.015	86
BM1				2.408 ± 0.017	86		2.507 ± 0.016	89
BM2				2.144 ± 0.005	**77**		2.175 ± 0.018	78
BM3				2.250 ± 0.006	82		2.345 ± 0.005	85
ICIE16				2.454 ± 0.015	**88**		2.440 ± 0.033	**88**
B1				2.580 ± 0.017	93		2.526 ± 0.011	91
B2				2.494 ± 0.021	92		2.579 ± 0.024	96
B3				2.550 ± 0.019	92		2.582 ± 0.018	93
BP1	750	10	60	2.567 ± 0.022	92	120	2.616 ± 0.017	94
BP2				2.509 ± 0.024	90		2.604 ± 0.005	93
BP3				2.589 ± 0.017	92		2.576 ± 0.005	91
BM1				2.590 ± 0.023	92		2.658 ± 0.028	95
BM2				2.549 ± 0.034	91		2.577 ± 0.005	92
BM3				2.582 ± 0.026	94		2.625 ± 0.028	95
ICIE16				2.419 ± 0.006	87		2.515 ± 0.085	90
B1	800	10	60	2.520 ± 0.013	94	120	2.590 ± 0.025	94
B2				2.546 ± 0.005	94		2.600 ± 0.030	96
B3				2.597 ± 0.006	93		2.640 ± 0.031	95
BP1				2.592 ± 0.027	93		2.634 ± 0.033	94
BP2				2.561 ± 0.025	91		2.512 ± 0.021	89
BP3				2.609 ± 0.009	92		2.580 ± 0.025	91
BM1				2.530 ± 0.005	90		2.585 ± 0.038	92
BM2				2.613 ± 0.011	94		2.680 ± 0.053	96
BM3				2.574 ± 0.014	94		2.576 ± 0.045	93

Increasing the heating rate to 20 K/min up to 700 °C and 750 °C led to large variation in the density. Fig. 2c shows that the yield density is above 73 % for BP1, BP2, BP3, BM1, BM2 and BM3. ICIE16 and B1 have approximately 87 % yield density, while B2 reached a density of 82 %. At 750 °C for the same heating rate, the density increased to more than 92 %, with the exception of BP1 glass, which reached a density of 96 % (Fig. 2d). Higher heating rates will enhance the glass flow only if the maximum sintering temperature of 800 °C is also exceeded to some extent; owing to the logarithmic dependence of the glass viscosity on the temperature, even a small degree of overheating will enhance the viscous flow considerably.

Increasing the dwell time at such a temperature up to 120 min has a low effect on the densification, because the glass flow has been impeded by the new crystallites. The density values at this dwell time are listed in Table 1.

(2) Phase identification

Fig. 3 shows the X-ray diffraction patterns of the samples sintered in 60 min dwell time and at a heating rate of 10 K/min at 700 (Fig. 3a), 750 (3b) and 800 °C (3c) respectively. It also shows the XRD patterns for glasses sintered at 750 °C in 60 min dwell time and at a heating rate of 20 K/min (Fig. 3d). After sintering at 700 °C, most of the sintered glasses kept their amorphous structure, except B2 and BP2 which exhibit broad peaks at 2θ of 20°. The broad peaks indicate that nanocrystals have formed with a size of around 45 nm.

After sintering at 750 °C all the glasses were crystallized, except for BP1, BM2 and BM3, which were still amorphous. The phases that mainly formed are $Na_4Ca_4Si_6O_{18}$, SiP_2O_7 and Ca_2SiO_4. The crystal sizes were calculated to be approximately 187 nm. Fig. 3c shows that after sintering at 800 °C all the glass have been crystallized to a certain extent depending on their chemical composition. While at 750 °C and at a heating rate of 20 K/min (Fig. 3d), BP1, BM2, and BM3 glasses remained amorphous, the other compositions have crystallized. In fact, there is no big difference in the XRD spectra among the glasses in Fig. 3b and 3d. The only difference can be seen in the yield density (Table 2).

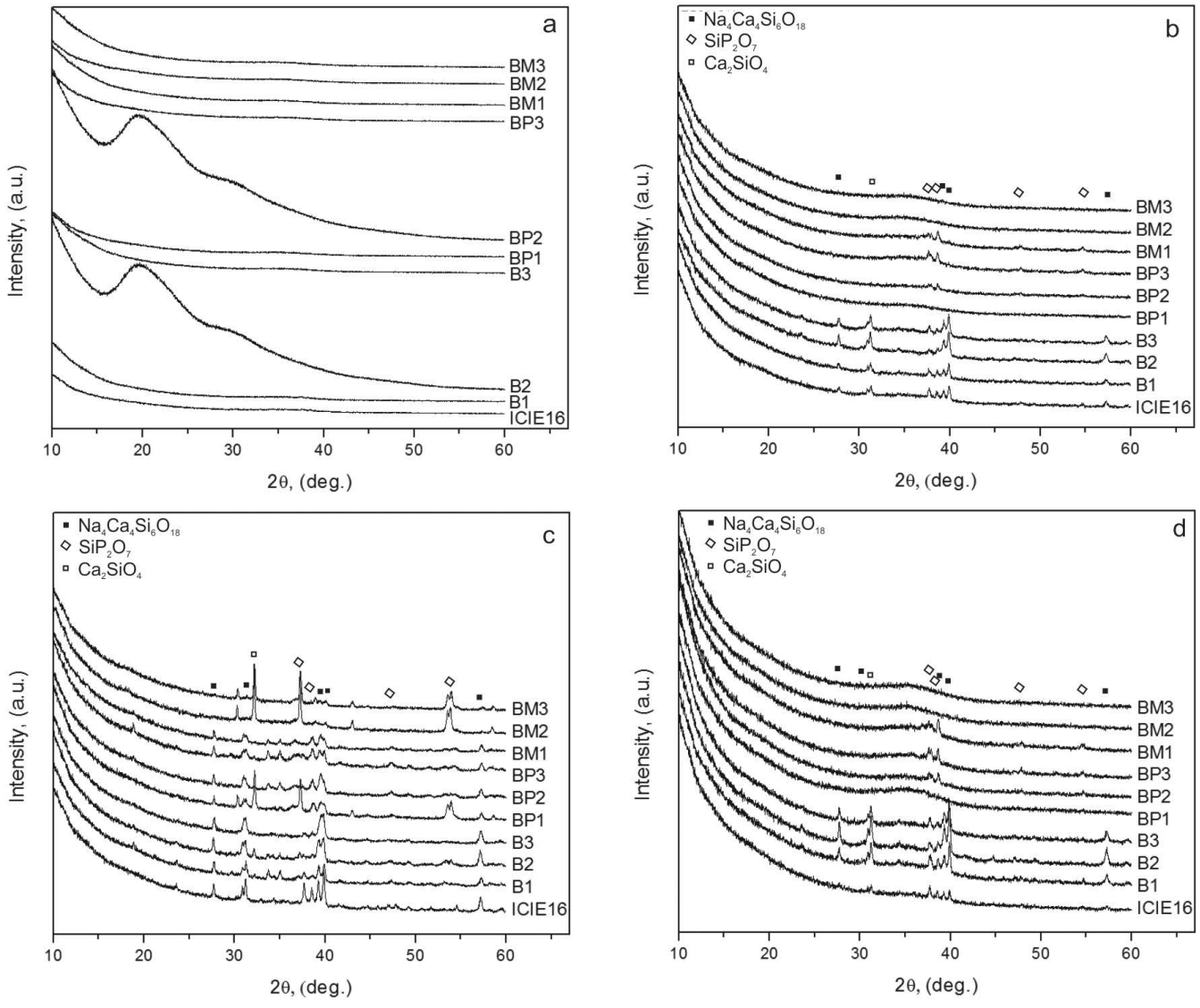

Fig. 3: X-ray diffraction patterns of the bioactive glasses sintered in different sintering conditions. a) sintered at 700 °C / 10 Kmin-1 / 60 min; b) 750 °C / 10 Kmin^{-1} / 60 min; c) 800 °C / 10 Kmin^{-1} / 60 min; d) 750 °C / 20 Kmin^{-1} / 60 min.

Table 2: Results of density at heating rates of 10 K/min, 20 K/min and at a soaking time of 60 min.

BG	T_{sin}, °C	Heating rate, K/min	Dwell time, min	Density, g/cm^3	density, %	Heating rate, K/min	Density, g/cm^3	density, %
ICIE16				2.396 ± 0.040	86		2.460 ± 0.024	**88**
B1				2.478 ± 0.015	90		2.249 ± 0.040	**88**
B2				2.492 ± 0.015	92		2.161 ± 0.023	83
B3				2.342 ± 0.021	84		2.095 ± 0.025	78
BP1	700	10	60	2.475 ± 0.012	89	20	2.069 ± 0.040	75
BP2				2.327 ± 0.010	83		2.074 ± 0.013	74
BP3				2.302 ± 0.005	82		2.102 ± 0.035	73
BM1				2.408 ± 0.017	86		2.153 ± 0.024	75
BM2				2.144 ± 0.005	**77**		2.001 ± 0.017	**77**
BM3				2.250 ± 0.006	82		2.172 ± 0.030	73
ICIE16				2.454 ± 0.015	**88**		2.511 ± 0.010	90
B1				2.580 ± 0.017	93		2.608 ± 0.050	94
B2				2.494 ± 0.021	92		2.551 ± 0.030	94
B3				2.550 ± 0.019	92		2.546 ± 0.032	91
BP1	750	10	60	2.567 ± 0.022	92	20	2.680 ± 0.035	96
BP2				2.509 ± 0.024	89		2.595 ± 0.030	92
BP3				2.589 ± 0.017	92		2.555 ± 0.040	90
BM1				2.590 ± 0.023	92		2.533 ± 0.020	90
BM2				2.549 ± 0.034	91		2.569 ± 0.030	92
BM3				2.582 ± 0.026	94		2.563 ± 0.021	93

(3) Microstructure

Fig. 4 shows SEM images of sintered glass samples. Neck formation at an early stage of the heat treatment (here at 650 °C) is clearly visible (Fig. 4a), which indicates the start of the sintering process. In addition, well-interconnected pores can still be seen in the same sample (Fig. 4a). This image supports the results of the density measurements (Table 1), where BM3 in these heat treatment conditions has reached a density of about 73 %. Increasing the sintering temperature has increased the glass flow and densification of the samples.

Although residual pores can be seen in Fig. 4b – 4d after the heat treatment has finished at 750 °C, these pores are isolated and not connected. It is noticeable that the fracture surfaces are smooth without visible grain boundaries. Fig. 4c shows a micrograph of a fracture surface for BP1 glass sintered at 750 °C for 60 min and at a heating rate of 20 K/min. This sample has a density of 96 %. The micrograph of BM2 in Fig. 4d exhibits residual pores but no grain boundaries. However, grain boundaries can be seen on a polished micrograph of BM2 glass (Fig. 5b). This glass has density of 92 % at 750 °C, 20 K/min for 60 min. Fig. 5b also shows that the residual pores are located mostly along the grain boundaries. While the micrograph of the BP1 sample sintered with the same sintering parameters (Fig. 5a) does not show clear grain boundaries, which implies a well-densified glass (96 % density).

It can be concluded from the density measurements and micrographs of fracture surfaces, that such heat treatments (i.e. pressureless sintering) are not enough to close all the residual porosity. Therefore, post heat treatment like hot isostatic pressing (HIP) would be necessary to eliminate them.

IV. Discussion

High-density sintered bioactive glass is of interest for different medical applications. Early crystallization of glass particles is considered the main reason for the low density of sintered bioactive glasses [12]. The problem is related to the glass network strength, i.e. whether the glass network bond is strong enough at the processing temperatures. As this is mostly related to the silica content, low silica content increases crystallization, which in turn reduces the bioactivity [13,14]. However, low silica content is also required to achieve high bioactivity. An amorphous microstructure makes bioactive glasses more dissoluble, which is not favorable, since it leads to burst release and basic pH in the supernatant surrounding the glass. Basic pH can have cytotoxic effects on the surrounding cells and tissue. This can be moderated by crystallization especially in static environments [15]. Therefore, a very controlled microstructure allows the production of bioactive glass-ceramics with moderate bioactivity and higher mechanical strength than amorphous bioactive glasses [16]. To achieve such microstructure, controlled heat treatment would be very important.

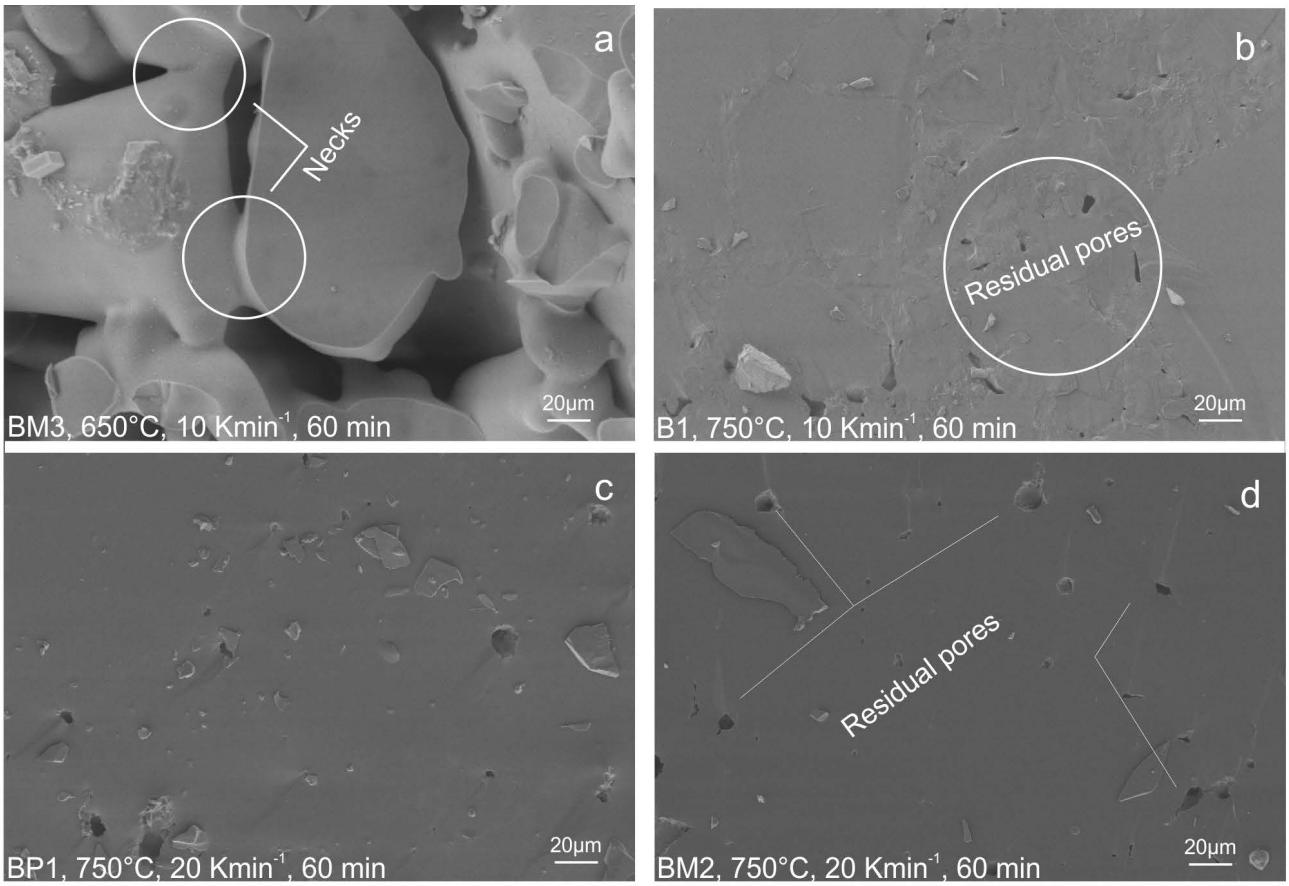

Fig. 4: SEM images of fracture surfaces coated with carbon. Neck formation and residual pores appear on the images for different glass compositions and temperature treatments.

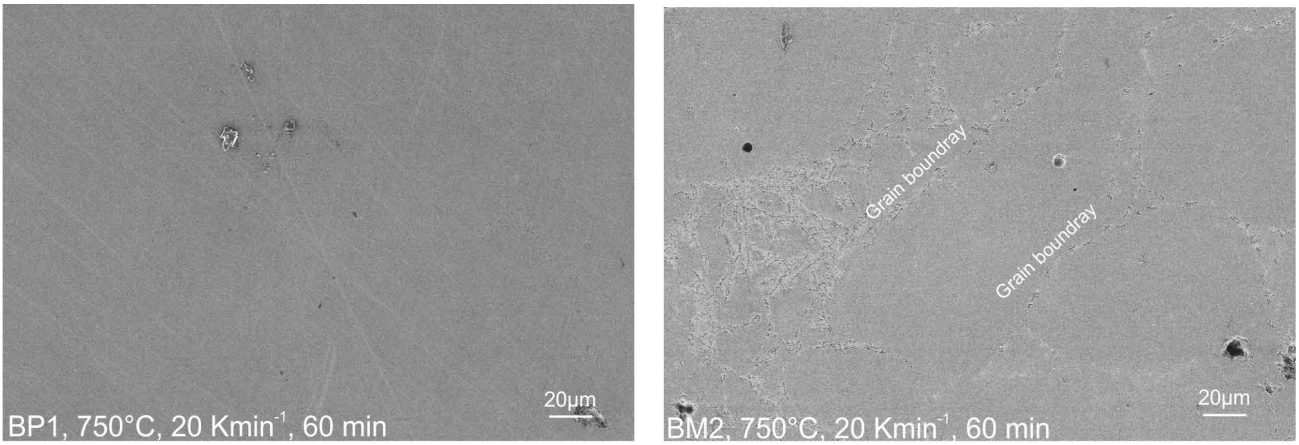

Fig. 5: SEM images of polished surfaces coated with carbon. Grain boundaries and residual pores are visible on the polished surfaces. a) No grain boundaries appeared; b) Visible grain boundaries.

Sintering temperature was determined based on the results of the hot-stage microscope analysis. In fact, the DTA analysis led to slightly different characteristic temperatures (glass transition and crystallization temperatures) than the heating microscope, although the particle size used in both investigations was 88 µm. This can be attributed to the difference in the sensitivity of the two devices (DTA and heating microscope). Similar results were also reported elsewhere in Reference [18]. To our knowledge, there is little information about sintering of ICIE16 glass. Wu *et al.* reported that the best sintering conditions for the ICIE16 bioactive glass are 700 – 710 °C at a dwell time of 60 min. They also reported that sintering at 730 °C led to quick crystallization. However, more information about the sintering behavior of ICIE16 has not been reported [6]. Sintering of 45S5 Bioglass® exhibits two shrinkages windows. The first is at 500 – 600 °C and the second one is at 850 – 1 100 °C. 45S5 Bioglass® starts to crystallize at 500 °C. This means that the yielded densification at the end of the first shrinkage is quite low, as sintering mostly stops after the first shrinkage until the second shrinkage is reached at temperatures above 850 °C [17]. ICIE16, in our study, has also showed two shrinkages (Fig. 1a): the first starts at around 675 °C and the second begins at around 1 075 °C. In comparison to ICIE16 and 45S5, all the developed glasses in this study

show one main shrinkage in the sintering window which continues until ~ 810 °C is reached (Fig. 1a).

With regard to our glasses, and as shown in Fig. 1, they start to flow at around 685 °C and flow ends at different temperatures depending on the chemical composition. Densification of B1 and B2 glasses finishes at ~ 780 °C, and for the other glasses (B3 to BM3) it finishes at ~ 810 °C. Therefore, depending on the composition, the developed glasses showed two sintering windows: B1 and B2 glasses had a sintering window of 95 °C, while the rest of the glasses showed a larger window of about 125 °C. We found that increasing the sintering temperature to 800 °C with a dwell time of 60 min and a heating rate of 10 $Kmin^{-1}$ leads to partial crystallization of all the investigated glass compositions (Fig. 3c). The findings have also shown that increasing the sintering time up to 120 min at a heating rate of 10 K/min has not increased the density to more than 95 %.

On the other hand, a higher heating rate provides more time for the glass to flow as crystallization is kinetically delayed. Increasing the heating rate up to 20 $Kmin^{-1}$ has increased the densification. However, the crystalline phases have not changed, as indicated by the XRD patterns (Fig. 3b and 3d) of the sintered bodies. BP1 sintered at 750 °C with a dwell time of 60 min showed the highest density of all samples with around 96 % when sintered at a heating rate of 20 $Kmin^{-1}$ (Fig. 2d). The phases formed were $Na_4Ca_4Si_6O_{18}$, SiP_2O_7 and Ca_2SiO_4. When we compare BP1 and ICIE16, the latter achieved just 90 % density with 20 $Kmin^{-1}$ at 750 °C with a partially crystalline microstructure. While the corresponding XRD pattern of BP1 glass (Fig. 3d) revealed that this glass retained an amorphous structure after the sintering in the same conditions. This means that increasing P_2O_5 content by 1 mol% besides introducing 1 mol% boron to ICIE16 have changed its sintering response as evidenced by the BP1 glass. BM2 and BM3 also retained their amorphous structure while achieving lower densification at 750 °C than BP1 (see Fig. 2 and Fig. 4).

From the results, we can infer that the chemical modifications, as declared in Reference [5], have led to an improvement in the sintering tendency of the yield glasses. When we look at the first group of glasses (B), it is noticeable that boron addition has not strengthened the glass network, as they crystallized at 750 °C, just like ICIE16. FTIR results in our previous investigations [5] indicated that most of the boron exists in threefold coordination, which indicates that boron is not incorporated into the silica network. This can lead to a weakened glass network and hence facilitate crystallization. However, the FTIR results also revealed a spectral feature, which could be associated to a fourfold coordination. Reducing the sodium content of 1 mol% while introducing boron into the glass network increased the glass network crosslinking, which in turn increased viscosity at the sintering range.

Increasing the phosphorous pent oxide (P_2O_5) content up to 2 % at the expense of sodium oxide strengthened the glass network in the series denoted BP glasses. This is apparent in BP1, as it kept its amorphous structure at 700 and 750 °C sintering temperature. BP2 and BP3, on the contrary, crystallized at 750 °C sintering temperature, which can be attributed to the increasing boron content up to 3 % in these glasses. In the third group denoted BM, the influence of magnesium oxide was investigated. BM2 and BM3 retained their amorphous structures after sintering at 700 and 750 °C and at both heating rates, i.e. 10 and 20 $Kmin^{-1}$, while BM1 crystallized after sintering at 750 °C. This behavior was anticipated since MgO maintains the silica network. Yet the high sintering temperature did not improve the densification of this glass group. It was considered here that MgO works as network modifier. More information about the structural aspects of the prepared glasses will be discussed in a separate study.

The SEM microstructures support the idea of viscous flow sintering, as at 700 °C sintering necks formed between the glass particles. In addition not all the grain boundaries disappeared during the sintering process, which is clearly seen in Fig. 5b. This was notable for BP1, BM2 and BM3 glasses. Li *et al.* succeeded in fabricating dense 45S5 Bioglass compacts using a spark plasma machine. The starting particle size was 9.8 μm. Combining small particle size and pressure during sintering can achieve densification at low temperatures around 423 °C with short dwell time of 3 min at a high heating rate of 50 $Kmin^{-1}$. The sintering pressure was 7.6 MPa. The yield samples had densities near to 100 % [18]. In another study, residual porosity was eliminated by means of post heat treatment using a hot isostatic pressing machine. The resulting glass (ZnO-B_2O_3-Bi_2O_3) was transparent at the end of the treatment. This glass was fabricated by means of pressureless sintering at 500 °C for 2 h and was hipped at 490 °C for 15 h. The maximum yield density was 98.8 % and the glass was transparent in the visible light range [19].

V. Conclusions

The sinterability and the sintering behavior of chemically modified ICIE16 bioactive glass have been discussed in this article. Adjusting the sintering parameters has improved the sinterability of the modified ICIE16 by reducing the crystallization tendency. The results have also revealed that a higher heating rate leads to more densification than the lower heating rate. BP1, which was sintered at 750 °C, 20 K/min for 60 min dwell time, showed the highest density of around 96 %. The X-ray diffraction patterns showed that this glass retained its amorphous structure after the heat treatment had been completed. This means a higher heating rate reduces the relaxation and the crystallization tendency in the glass and therefore allows more viscuos flow during sintering. SEM micrographs revealed smooth surfaces without visible grain boundaries (Fig. 5a). In other glass compositions and at higher sintering temperatures the resulting crystalline phases in the glasses were identified as $Na_4Ca_4Si_6O_{18}$, SiP_2O_7 and Ca_2SiO_4.

References

[1] Jones, J.R., Lin, S., Yue, S., Lee, P.D., Hanna, J.V., Smith, M.E., *et al.*: Bioactive glass scaffolds for bone regeneration and their hierarchical characterization, *Proc. Mech. Eng. Part H: J. Eng. Med.*, **224**, 1373 – 1387, (2010).

[2] Rahaman, M.N., Day, D.E., Bal, B.S., Fu, Q., Jung, S.B., Bonewald, L.F., *et al.*: Bioactive glass in tissue engineering, *Acta Biomater.*, **7**, 2355 – 2373, (2011).

3 Elgayar, I., Aliev, A.E., Boccaccini, A.R., Hill R.G.: Structural analysis of bioactive glasses, *J. Non-Cryst. Solids, **315**, 173 – 183, (2005).*

4 Groh, D., Döhler, F., Brauer, D.S.: Bioactive glasses with improved processing. part 1. thermal properties, ion release and apatite formation, *Acta Biomater.*, **10**, 4465 – 4473, (2014).

5 Hmood, F., Goerke, O., Schmidt, F.: Chemical composition refining of bioactive glass for better processing features, part I, *Biomed. Glasses, **4**, 82 – 94, (2018).*

6 Wu, Z.Y., Hill, R.G., Jones, J.R.: Optimizing the processing of porous melt-derived bioactive glass scaffolds, *Bioceram. Dev. Appl.*, **1**, 1 – 4, (2011).

7 Hmood, F., Guenster, J., Heinrich, J.G.: Sintering and piezoelectric properties of $K_{0.5}Na_{0.5}NbO_3$ glass microspheres, *J. Eur. Ceram. Soc., **35**, 4143 – 4151, (2015).*

8 Wadsworth, F.B., Vasseur, J., Llewellin, E.W., Schauroth, J., Dobson, K.J., Scheu, B., *et al.*: Sintering of viscous droplets under surface tension, *Proc. R. Soc.*, **A472**, 20150780, (2016).

9 Cutler, I.B.: Sintering of glass powders during constant rates of heating, *J. Am. Ceram. Soc., **52**, 14 – 17, (1969).*

10 Agea-Blanco, B., Reinsch, S., Müller, R.: Sintering and foaming of barium silicate glass powder compacts, *Front. Mater.,* **3**, 45, (2016).

11 Zanotto, E.D.: Glass crystallization research — A 36-year retrospective. part I, fundamental studies, *Int. J. App. Glass Sci.*, **4**, 105 – 116, (2013).

12 Boccaccini, A.R., Stumpfe, W., Taplin, D.M.R., Ponton, C.B.: Densification and crystallization of glass powder compacts during constant heating rate sintering, *Mater. Sci. Eng., **A219**, 26 – 31, (1996).*

13 Lefebvre, L., Gremillard, L., Chevalier, J., Zentai, R., Bernache-Assolant, D.: Sintering behavior of 45S5 Bioglass®, *Key Eng. Mat.*, **361**, 265 – 268, (2008).

14 Cormack, A.N., Tilocca, A.: Structure and bioactivity of glasses and ceramics, *Philos. T. R. Soc. A, **370**, 1271 – 1280, (2012).*

15 Ciraldo, F.E., Boccardi, E., Melli, V., Westhauser, F., Boccaccini, A.R., Tackling bioactive glass excessive in vitro bioreactivity: Preconditioning approaches for cell culture tests, *Acta Biomater.*, **75**, 3 – 10, (2018).

16 Gerhardt, L., Boccaccini, A.R.: Bioactive glass and glass-ceramic scaffolds for bone tissue engineering, *Materials*, **3**, 3867 – 3910, (2010).

17 Li, Z., Thompson, B.C., Hu, H., Kohr, K.: Rapid fabrication of dense 45S5 Bioglass® compacts through spark plasma sintering and evaluation of their in vitro biological properties, *Biomed. Mater.,* **11**, 065006, (2016).

18 Bretcanu, O., Chatzistavrou, X., Paraskevopoulos, K., Conradt, R., Thompson, I., Boccaccini, A.R.: Sintering and crystallization of 45S5 Bioglass® powder, *J. Eur. Ceram. Soc.*, **29**, 3299 – 3306, (2009).

19 Abe, K., Hamada, J., Miyazawa, M., Kuwahara, H., Itatani, K.: Fabrication of transparent sintered $ZnO\text{-}B_2O_3\text{-}Bi_2O_3$ glass body by pressureless firing and hot isostatic pressing, *IOP Conf. Ser.: Mater. Sci. Eng.*, **47**, 012024, (2013).